# Fixed-bed reactors for exothermic reactions: A qualitative relation between start-up time and traveling waves velocity

Axel Fache, Frédéric Marias, Marco Castaldi, Michael Lugo-Pimentel, Yegor Nikitin, Tasnuva Moutushi

# Fixed-bed reactors for exothermic reactions: a qualitative relation between start-up time and traveling waves velocity.

Axel Fache, Laboratoire de Thermique Energétique et Procédés – IPRA EA1932, Université de Pau et des Pays de l'Adour/E2S UPPA, 64000 Pau, France

Frédéric Marias, Laboratoire de Thermique Energétique et Procédés – IPRA EA1932, Université de Pau et des Pays de l'Adour/E2S UPPA, 64000 Pau, France

Marco J. Castaldi, City University of New York, City College, Dept. of Chemical Engineering, New York, NY, USA

Michael Lugo-Pimentel, City University of New York, City College, Dept. of Chemical Engineering, New York, NY, USA

Yegor Nikitin, City University of New York, City College, Dept. of Chemical Engineering, New York, NY, USA

Tasnuva Moutushi, City University of New York, City College, Dept. of Chemical Engineering, New York, NY, USA

**Abstract**

An experimental investigation of the reaction front movements upon reacting gas injection in a pre-heated non-adiabatic fixed-bed methanation reactor is conducted. The relocation starts with a backward movement of the front, whose maximal velocity turns out to be a linear function of the temperature setpoint. The front then moves forward in response to the fact that the injected cold gas cools down the bed in the upstream zone. The front stabilizes asymptotically in the downstream (upstream, resp.) zone of the reactor after a characteristic time that is an increasing (decreasing, resp.) function of the temperature setpoint, if the setpoint is below (above, resp.) a certain threshold. This behavior is interpreted in terms of reaction wave velocity.

**Keywords:** fixed-bed reactor; start-up time; exothermic reaction; wave propagation; reaction front velocity

**Notations :**

| Symbol | Quantity, unit |
|---|---|
| $C_p$ | Constant pressure heat capacity, $J.kg^{-1}$ |
| $\dot{Q}_{ext}$ | Volumetric thermal power transferred from the external medium to the reactor, $W.m_{medium}^{-3}$ |
| $\dot{Q}_{reac}$ | Volumetric power released by the reaction (exothermicity), $W.m_{medium}^{-3}$ |
| $\dot{Q}_{sens}$ | Volumetric power advection due to gas movement, $W.m_{medium}^{-3}$ |
| $\dot{r}$ | Volumetric reaction rate, $mol.m_{medium}^{-3}.s^{-1}$ |
| $T$ | Reaction medium temperature, $°C$ |
| $t$ | time, $s$ |
| $T_{ext}$ | Temperature of the external medium (furnace), $°C$ |
| $T_{set}$ | Setpoint temperature, $°C$ |
| $T_{thres}$ | Threshold setpoint temperature, $°C$ |
| $T_{1/2}$ | Local characteristic time, $s$ |
| $v_{chem}$ | Chemically-induced wave velocity, $m.s^{-1}$ |
| $v_{ext}$ | Wave velocity due to the heat exchange with the external medium (furnace), $m.s^{-1}$ |
| $v_{gas}$ | Gas interstitial velocity , $m.s^{-1}$ |
| $v_{hot}$ | Hotspot velocity, $m.s^{-1}$ |
| $v_{hot/T}$ | Hotspot velocity, relative to an isothermal point, $m.s^{-1}$ |
| $v_T$ | Isothermal point velocity, $m.s^{-1}$ |
| $v_{therm}$ | Thermal wave velocity, $m.s^{-1}$ |
| $z$ | Axial location, $m$ |
| **Greek letters** | |
| $\Delta_r H$ | Reaction enthalpy, $J.mol^{-1}$ |
| $\delta X$ | Small element of quantity $X$ (> 0 by default) |
| $\rho$ | Density, $kg.m_{medium}^{-3}$ |
| $\tau$ | Characteristic time of the equivalent exponential function, $s$ |
| **Subscript** | |
| $ad$ | Adiabatic |
| $front$ | Relative to the reaction front (generic for isothermal point or hotspot) |
| $hot$ | Hotspot |
| medium | Relative to the reaction medium {porous solid + gas} |
| $set$ | At the same temperature as the setpoint |
| $T$ | For a point whose temperature is $T$ (isothermal point in Lagrangian description) |
| **Superscript** | |
| $min$ | When the front reaches its lower axial position. |
| $\infty$ | Asymptotic value |

## 1. Introduction

### 1.1. General context

The transient behavior of fixed-bed catalytic reactors dedicated to exothermic reactions is a subject of interest in many regards [1], whether the reactor is intended to complete the reaction dynamically (e.g. methanation reactors dedicated to power-to-gas [2, 3]), or not (safety issues after accidental perturbations of the operation conditions, or normal start-up of the reactor [4]). Due to the difference between the characteristic time of the gas movement through the reactor and the characteristic time of the thermal phenomena, transient behavior cannot be addressed as a succession of quasi steady states. Counter-intuitive phenomena can take place. Wrong-way behavior [5], for example, consists in a transient variation of local and global quantities (temperature, reaction rate, chemical yield, etc) that spontaneously reverses before stabilizing asymptotically, further to a dynamic perturbation in the operation conditions (e.g. inlet gas composition, flow rate or temperature). Many previous studies have examined the response of a reactor upon all sorts of such perturbations [6-10].

One way to apprehend the transient behavior of a reactor is to think in terms of waves that propagate in the downstream or upstream direction. This approach constitutes a powerful theoretical tool to understand and predict phenomena such as ignition point relocation, extinction, wrong-way behavior or transition between multiple steady states [11-17]. It can be used to describe how the periodic variation of operation parameters can be amplified in a similar manner as a resonance phenomenon [18, 19] with the further aim of controlling it. As summarized by Li et al. [20], the reversal of the flow can lead to trap the released heat in the reactor: the corresponding flow cycle characteristic time is related to the velocity of the thermal wave propagation.

Transient phenomena can also be exploited to operate a reactor system more safely and efficiently under well controlled variable conditions than under stable steady-state conditions [18, 21], which the wave propagation theory successfully describes. For example, Altimari et al. [21] considered the case of loop reactors dedicated to methanol synthesis to show that the competition between the

respective velocities of rising and declining temperature fronts impacts the range of switch times that are compatible with stable operation.

### 1.2. Scope of the study

The present study concerns the start-up of a catalytic methanation reactor:

$CO_2 + 4 \cdot H_2 \rightleftharpoons CH_4 + 2 \cdot H_2O, \Delta_r H^0 = -165\ kJ/mol_{CO2}$.

This reaction has been attracting much research interest over the past five years, due to its potential interest for renewable energy conversion and storage [22].

A previous research effort was made to numerically characterize the start-up time [23] when a reacting gas is suddenly injected in a warm reactor. The aim of the present experimental work is to examine the reaction front movement from the initial state (idle state – warm bed with no gas injection) to the nominal steady state (constant gas flow rate after a step injection).

The experimental setup and procedure are described in part 2, together with the data processing that will be performed to access the desired information.

It should be mentioned that the catalyst used in the present study was based a novel processing technology for producing thin, nanostructured Ni coatings on metal substrates. The coatings are interdiffused enabling intimate connectivity between the active elements for reaction and the base substrate, resulting in mechanical robustness. This results in a catalytic element that is approximately 100 µm thick providing a unique advantage for methanation (or for steam methane reforming) at high space velocities.

The results presented in part 3 are interpreted from a wave propagation point of view. To the authors' knowledge, the wave propagation theory has never been used to describe the evolution of the start-up time itself (characteristic time required for the front to reach its steady-state location). This topic however appears interesting because the start-up time actually is related to the wave velocities variations. The gradual cancellation of the front velocity is indeed a synonymous with the eventual front stabilization. The present work fills this gap by establishing a bridge between the start-up time assessment and the wave propagation theory. Only the axial propagation aspects are of

interest: the examination of advanced phenomena (e.g. transversal hotspot formation [24, 25] or microscopic/macroscopic mechanisms coupling [26]), are beyond the scope of this study. Yet prior to discussing the system configuration and results it is important to review propagation of transient behavior in catalytic reactors.

### 1.3. Wave propagation theory – technical aspects

The wave propagation theory consists in following the position $z_T$ of a reaction front point whose temperature is $T$ (Lagrangian description: $z_T$; $T(z_T) = constant$): this point moves at velocity $v_T = dz_T/dt$.

If the gas flows through the bed at interstitial velocity $v_{gas}$, a thermal perturbation will propagate in the same direction as the gas (forward movement) with a characteristic velocity $v_{therm}$:

$$v_{therm}(z_T, t) = \frac{\rho^{gas} \cdot C_p^{gas}}{\rho^{solid} \cdot C_p^{solid} + \rho^{gas} \cdot C_p^{gas}} \cdot v_{gas}(z_T, t) \text{ (Eq. 1)}$$

The densities used in equation 1 are apparent and therefore incorporate the void fraction. $\rho \cdot C_p$ is the heat capacity of the corresponding medium (solid or gas) per unit of reaction medium (solid+gas) volume.

If the axial conduction through the porous solid that constitutes the bed is significant, a conduction thermal wave can also be introduced. The reaction front in an adiabatic reactor can therefore move in the opposite direction of the gas flow (backward movement), when cold gas is injected in a cold bed and the reaction is ignited in a downstream portion of the bed by a local external heating. Conduction enables the thermal power released by the reaction to be dispersed in both direction (upstream and downstream), but since the reactants are purer in the upstream part of the reaction front, ignition takes place in a more and more upstream axial location [7] (until an equilibrium is reached). Vortmeyer & Jahnel [27] summarized this observation as follows:

*"The movement against the flow is the most interesting feature and can only be explained by axial diffusion processes of heat and mass"*. It should be emphasized that this statement corresponds to a situation where the bed is initially cold. In this situation indeed, the reaction doesn't initially occur in

the upstream zone of the bed, and axial conduction is necessary for the upstream zone to heat-up via the above-described mechanism.

If the gas is injected through a bed whose initial temperature is sufficient for the reaction to ignite in the whole reaction medium length (warm start), axial conduction is no longer a theoretical requisite for the reaction front to move against the flow. Due to the reaction all along the bed, the temperature tends to increase in all of the bed length immediately after the gas injection starts. Therefore, a point of the reaction front whose temperature is $T$ can move backward. The component associated to this phenomenon can be modeled as a propagating wave that moves at velocity $v_{chem}$:

$v_{chem}(z_T, t) = -\frac{\dot{Q}_{reac}(z_T,t)}{\dot{Q}_{sens}(z_T,t)} \cdot v_{therm}(z_T, t)$ (Eq. 2)

where $\dot{Q}_{reac}(z_T, t) = (-\Delta_r H) \cdot \dot{r}(z_T, t)$ is the volumetric power released by the reaction at location $z_T$ (per reaction medium volume)

and $\dot{Q}_{sens}(z_T, t) = \rho^{gas} \cdot C_p^{gas} \cdot \left(\frac{\partial T}{\partial z}\right)_{z_T,t} \cdot v_{gas}(z_T, t)$ is the net volumetric thermal power transported by the gas flow in the presence of a temperature gradient.

The presence of an external heat exchange term adds a third wave:

$v_{ext}(z_T, t) = -\frac{\dot{Q}_{ext}(z_T,t)}{\dot{Q}_{sens}(z_T,t)} \cdot v_{therm}(z_T, t)$ (Eq. 3)

with $\dot{Q}_{ext}(z_T, t)$ the thermal power transferred from the external system to the reaction medium, per unit of reaction medium volume.

In summary, the movement of an isothermal point results from the competition between these three components:

$v_T(z_T, t) = v_{therm}(z_T, t) + v_{chem}(z_T, t) + v_{ext}(z_T, t)$ (Eq. 4)

Equation 4 is fundamentally derived from a simplified reactor model (more details in appendix A). It can be understood qualitatively as follows:

- ignoring the external transfer, if the thermal energy released by the reaction is lower than the thermal energy required for the reaction medium to keep its temperature gradient, then the corresponding energy deficit leads to a decrease in the temperature of the front, and the

isothermal line moves forward. Conversely, if $\dot{Q}_{reac}/\dot{Q}_{sens}$ exceeds 1, the front increases in temperature, so the isothermal line moves backward.

- if one assumes a simple external heat transfer of the form $\dot{Q}_{ext} \propto T_{ext} - T$, then for a given external temperature $T_{ext}$, $v_{ext}$ is an increasing function of the local temperature $T$. To be more specific, $v_{ext}$ is positive (negative, resp.) if the external medium cools-down (heat-up, resp.) the reaction medium, and $|v_{ext}|$ is higher when $|T_{ext} - T|$ is higher. In other words, the external transfer generates a rotation of the reaction front to make it more parallel to the external medium axial temperature profile (horizontal profile if $T_{ext}$ is uniform).

Many variations of equations 1 to 4 can be derived. Zahn [28] adopted a simplified form for an adiabatic reactor, assuming that the reaction front is nearly linear and the reaction rate is uniform in space. This assumption makes sense as a first approximation, since the consumption of the reactants comes with a temperature increase (exothermicity): the two effects usually tend to oppose each other along the reaction front in an adiabatic reactor. Still, the two effects are non-linear and the assumption that they cancel each other, while convenient, is restrictive. In particular, if the conversion of a reactant fraction generates a temperature increase whose effect on the reaction rate is considerably stronger than the effect of the corresponding reactant rarefaction, the temperature at this location $z$ increases dramatically, and:

i) The downstream part of the reaction front is subject to a temperature increase that is higher at location $z$ than at location $z + \delta z$: $\left(\frac{\partial T}{\partial t}\right)_z > \left(\frac{\partial T}{\partial t}\right)_{z+\delta z} > 0$. The downstream part of the front slope hence decreases through time $\left((\partial^2 T/\partial t \partial z)_{z+,t} < 0\right)$.

ii) The upstream part of the front is subject to a temperature increase that is higher at location $z$ than at location $z - \delta z$: $\left(\frac{\partial T}{\partial t}\right)_z > \left(\frac{\partial T}{\partial t}\right)_{z-\delta z} > 0$. The upstream front slope gets steeper through time $\left((\partial^2 T/\partial t \partial z)_{z^-,t} > 0\right)$.

Conversely, if the conversion of a reactant fraction is such that the corresponding temperature increase is insufficient to keep the reaction rate at its current value, the temperature will drop locally. In both cases, the front velocity is strongly non-uniform.

## 2. Equipment and method

### 2.1. Experimental setup and procedure

The general setup is shown on figure 1. The tubular reactor made of Inconel-625 is 1 cm in internal diameter. The 20 cm long reaction medium consists of 1.53 g Nickel-based catalyst diluted in 28.7 g alumina. This diluted catalyst was loaded in the reactor under the form of 10 partial loads, in an effort to limit the risk of pellets segregation (table 1). More information about the catalyst properties is provided by Lugo-Pimentel [29]; the alumina pellets are 0.3 mm in average diameter. The inlet and outlet zones of the tube are filled with 6 g of alumina pellets each (corresponding to a length of 4 cm). Five type-K thermocouples of diameter 1.6 mm are used to measure the internal temperature of the reactor ($T_1$ to $T_5$) as illustrated on figure 2. The temperatures are recorded every 10 s. The electric furnace power is controlled in such a manner that $T_{set}$ is equal to the temperature setpoint. $T_{set}$ is measured in the narrow space between the reactor outer wall and the furnace inner wall, at $z = 14\ cm$ (middle axial location). The $z$ axis is horizontal to limit the consequences of natural convection on the temperature profile. Mass flow controllers Unit Instrument UFC-1100 are used for $H_2$ and $CO_2$ supply, and a Tylan FC-280S supplies $N_2$ as a tracer. The product gas composition is measured every 4 minutes by an Inficon series 3000 gas chromatograph.

Six experiments are performed, each one corresponds to a given $T_{set}$ (table 2). The experiments were carried out in the following chronological order: 2, 5, 1, 6, 4. This randomization constitutes a precaution against the eventuality of a gradual catalyst deactivation effect, although previous work using this catalyst didn't find any deactivation in the range of temperatures here explored. The intermediate temperature corresponding to experiment #3 was added to the initial plan because the preliminary observations of the results showed that the range between 400°C and 420°C deserved extra attention (see part 3).

For each experiment, the reactor is heated without any fluid flow for a duration of 5 hours in order to make sure that the thermal idle steady state is reached. During this heat-up phase, the reactor contains pure $H_2$ in order to preserve the catalyst. A gas mixture that consists of $CO_2/H_2/N_2$ 200/800/20 mL(STP)/min is then injected in the reactor (step injection – instant $t = 0$ is the instant when the gas valve is opened). The gas is supplied at 22°C, and the reactor outlet pressure is 5 bar. The gas injection is maintained for a minimum duration of 2 hours. The furnace remains operative and controlled at $T_{set}$ during the whole experiment. The authors stress that even though the furnace keeps on delivering some heat after the gas injection step, the reactor itself can be hotter than the furnace in most of the reactor length ($\dot{Q}_{ext} < 0$): the furnace power compensates the thermal loss that exceeds the reaction exothermicity. Such high thermal loss would not be representative of practical industrial situations, where scale effects imply low relative thermal loss (low system outer surface area / reaction volume ratio).

### 2.2. Post-treatment

The post-treatment procedure is summarized figure 3. On the basis of the recorded temperatures, a 4$^{th}$ degree polynomial interpolation is built at each instant (figure 4). This polynomial interpolation is used to calculate the location of the isothermal point $z_T$ for each experiment, at each instant:

$z_T(t);\ T(z_T, t) = T_{set}\ with\ (\partial T/\partial z)_{T_{set}} > 0$ (Eq. 5)

Note that the positive space derivative means that the considered isothermal point is on the reaction front (transition between the non-ignited zone with a low-temperature, and the ignited zone with a higher temperature).

The maximum of the interpolation function is called “hotspot” in the sequel. The authors strongly emphasize that the real hotspot can be different from this interpolation-based hotspot. Rather than an accurate prediction of the real hotspot properties, the aim of the interpolated hotspot is to indicate the axial zone where the reaction is the most active. Indeed, the most active zone corresponds to a gradual change in the sign of the temperature space-derivative: the interpolated hotspot location $z_{hot}$ is a signature of this reversal.

The reaction front movement will be assessed through the evolution of both $z_T(t)$ and $z_{hot}(t)$. The generic notation $z_{front}(t)$ is used to indicate that the description used for the isothermal point represents $z_T(t)$ (i.e. $z_{front}(t) = z_T(t)$), yet for the case of the hotspot it is $z_{hot}(t)$ (i.e. $z_{front}(t) = z_{hot}(t)$).

Preliminary experiments have shown that the gas injection implies a wrong-way behavior that can be broken down into two steps (qualitative illustration on figure 5). Each step will therefore lead to an analysis as described hereafter, together with an interpretation of the obtained results in terms of wave propagation velocity.

#### 2.2.1. Step 1

The hotspot is initially located in the middle of the reactor (axial hotspot before gas injection, due to border effects). The isothermal point $z_T$ can't be defined at $t = 0$, because the temperature of any point of the reactor at $t = 0$ is slightly lower than $T_{set}$ ($T_{set}$ is controlled in the furnace). However the reaction enables $z_T$ to be defined as soon as the reaction starts, and the first defined value of $z_T$ is close to 14 cm.

The first step of the reaction front relocation consists in a quick backward movement (figure 5). During this step, the strongest value of the front velocity $\max(|v_{front}(t)|)$ will be calculated (equation 6) for each experiment, in order to assess the effect of the setpoint temperature on this upstream-oriented movement.

$v_{front}(t) = \frac{z_{front}(t+\delta t) - z_{front}(t)}{\delta t}$ with $\delta t = 10\ s$ (Eq. 6)

#### 2.2.2. Step 2

The front moves slowly towards the outlet. The characteristic time for the front to move from $z_{front}^{min}$ to its asymptotic value $z_{front}^{\infty}$ is the quantity of interest for this part. Indeed, $t^{min}$ is low so the characteristic time of the forward movement is a relevant indicator of the time it takes for the reactor to start-up. Defining a relevant characteristic time is not straightforward, because $z_{front}(t)$ does not correspond *a priori* to a simple usual mathematical function. Therefore, two different characteristic times are introduced for the $z_{front}(t)$ vs. $T_{set}$ response assessment (figure 5).

**i-** The first characteristic time will be referred to as "local characteristic time" $T_{1/2}$, defined according to equation 7. This definition if very simple, but the comparison of the $T_{1/2}$ values has a limited meaning if the different curves shapes aren't sufficiently similar to each other. Another difficulty is to determine the exact value of $z_{front}^{\infty}$ if steady state is still not totally reached after a few hours of experiment.

$T_{1/2}$ ; $z_{front}(T_{1/2} + t^{min}) = \frac{z_{front}^{\infty} + z_{front}^{min}}{2}$ (Eq. 7)

**ii-** The second characteristic time will be referred to as "integral characteristic time" $\tau$, it is defined according to equation 9. This relation is based on the following idea: if an inert cold gas was suddenly injected in a pre-heated furnace, then the thermal front would move forward. The time-dependent location of the thermal front would be equal to lower axial position and the additional distance required for the front to reach the asymptote, and the evolution of $\mathrm{z_{front}(t)}$ would theoretically follow a simple exponential law[1] (equation 8). The corresponding characteristic time $\tau$ could be determined according to equation 9. In the present case, the reaction implies that the evolution of $z_{front}(t)$ isn't theoretically exponential. In other words, the real situation (with reaction) is assessed through an equivalent theoretical (inert) situation. Although this approach is more complex than the local one, $\tau$ offers two advantages compared to $T_{1/2}$. First, due to its integral nature, it is more representative of the global evolution of the $z_{front}(t)$ curve: the comparison of two curves whose shapes are slightly different from each other remains possible through the equivalent function, and the unavoidable small local oscillations of $z_{front}$ tend to cancel statistically. Second, $z_{front}^{\infty}$ doesn't need to be known for the calculation of $\tau$: the calculation remains possible if the experiment approaches the steady state without totally reaching it.

From a practical point of view, the integral terms are determined by the trapezoidal rule, and successive values of $\tau$ are tested (dichotomy – stopping criterion: difference between successive

[1] Other ways of building the equivalent exponential law are discussed in appendix B. The various methods don't change much the value of $\tau$, and our conclusions about the effect of $T_{set}$ remain identical.

values < 10 s) until equation 9 is fulfilled.

$$z_{front}(t) \underbrace{=}_{assumption} z_{front}^{min} + (z_{front}^{\infty} - z_{front}^{min}) \cdot \left(1 - \exp\left(-\frac{t - t^{min}}{\tau}\right)\right) \text{ (Eq. 8)}$$

$\tau$ ; $A(\tau) = B(\tau)$ (Eq. 9)

with $A(\tau) = \left(\frac{(t^{\infty} - t^{min})}{2} + \tau \cdot \exp\left(\frac{t^{min} - t^{\infty}}{2 \cdot \tau}\right) - \tau\right) \cdot \int_{t^{min}}^{t^{\infty}} z_{front}(t) \cdot dt$

$$B(\tau) = \left(t^{\infty} - t^{min} + \tau \cdot \exp\left(\frac{t^{min} - t^{\infty}}{\tau}\right) - \tau\right) \cdot \int_{t^{min}}^{\frac{t^{\infty} + t^{min}}{2}} z_{front}(t) \cdot dt$$

$t^{\infty}$ is the duration of the experiment.

## 3. Results and discussion

### 3.1. General observations

The front position $z_{front}$ for the six experiments is shown on figure 6. After the sharp backward movement (step 1), it appears that the forward movement (step 2) can be strong or very weak, depending on the temperature setpoint of the furnace:

- At low temperature, the forward movement is large and the hotspot tends to stabilize in a downstream zone of the reactor ($z_{hot}^{\infty} > 14cm$). The chosen setpoints are however high enough to avoid a complete blow away of the reaction front.
- At high temperature, the front stays very close to $z_{front}^{min}$ and the hotspot remains confined in the upstream zone of the reactor. This arises from the exothermicity of the reaction that is further described in part 3.3.2.

We observe a transition at ~410°C but we cannot positively affirm if this transition takes the form of 2 zones of operation that are really distinct. There might exist a threshold temperature $T_{thres}$ (410°C < $T_{thres}$ < 420°C) that separates the two steady-state front stabilization behaviors. Yet it is known that multiple steady-states (depending on the operation history) and oscillating solutions can exist [17, 30]. Without capturing all temperature possibilities it is difficult to conclusively identify which prevails.

The conversion of $CO_2$ into methane as a function of time is reported on figure 7 (no conversion is calculated at t = 0 because the corresponding gas sample is similar to that contained in the reactor just before injection). The asymptotic conversion is approximately reached as early as t = 4 min (except for $T_{set} = 380°C$). A slight decreasing trend seems to be at stake long after t=4 min, which is consistent with the fact that it takes time for the reactor to reach its real steady state (long thermal transition). This trend is however low compared to the instant conversion fluctuations. Thus, from the first or second measurement (t=4min or t=8min) any possible variations in the outlet composition are too low to be detected there they are considered constant. In other words, the thermal power released by the reaction in the whole reactor can be deemed approximately constant for the whole duration of the experiment.

Parts 3.2 and 3.3 hereafter examine more specifically how the front movement can be related to propagating waves velocity.

### 3.2. Backward movement and transition to the forward movement

Figure 8 illustrates the backward propagation mechanism explained in part 1.3, in the typical case of $T_{set} = 410°C$: while $T_2$ is initially lower than $T_3$, $T_2$ increases faster than $T_3$. An isothermal point can therefore move backward. Since $(\partial T/\partial t)_{z_{hot}-\delta z} \gg (\partial T/\partial t)_{z_{hot}}$, the hotspot itself increases in temperature as it moves backward.

The maximum value of $|v_{front}(t)|$ during the first step is reported as a function of $T_{set}$ on figure 9. The relation between $v_{front}$ and $T_{set}$ turns out to be approximately linear. This observation echoes the results of previous studies, where the start-up time of a wall-cooled reactor was a quasi-linear function of its initial temperature [23], or where a front wave velocity was a quasi-linear function of the flow rate [15]. The present result shows another situation where a characteristic of a reactor's dynamic behavior is actually very simple, despite the fact that highly non-linear phenomena are fundamentally involved. We also have $|v_{hot}| < |v_T|$. The hotspot temperature increase tends to oppose the backward movement:

$v_{hot} = v_T + v_{hot/T}$ (Eq. 10)

with $v_{hot/T}$ the hotspot velocity in the reference frame of the isothermal point: $v_{hot/T} \approx \left(\frac{1}{\partial T/\partial z}\right)_{z_{hot}} \cdot \frac{dT_{hot}}{dt}$ if the hotspot temperature evolves along a linear reaction front.

The backward movement can be analyzed in terms of wave propagation velocity.

The value of $\dot{Q}_{sens}$ is initially low (low $\partial T/\partial z$ during the idle state): $\dot{Q}_{reac}/\dot{Q}_{sens} \gg 1$, hence the strong backward movement. The backward movement will end eventually as $\dot{Q}_{sens}$ increases up to $\dot{Q}_{react}$, due to two phenomena:

i- $\dot{Q}_{reac}$ itself generates a strong increase in $\partial T/\partial z$.

ii- The low temperature of the injected gas generates a cold thermal wave that reaches the low values of $z$ first.

It should be noticed that the gas velocity can be deemed approximately independent on the axial location and on the setpoint, because the methanation reaction generates a decrease in mole quantities (5 mol → 3 mol) while releasing heat. This simplifies the calculation of an order of magnitude for the thermal wave velocity. The (constant) flow rate used in experiments #1 to 6 and the typical values of the solid and gas properties in the reactor lead to a typical thermal wave velocity $v_{therm} \approx 10^{-4} m/s$ (constant). This value is one order of magnitude lower than the maximum value of $|v_{front}|$, which confirms numerically that the chemical wave is strongly preponderant during the fast backward movement ($v_{front} \approx v_{chem}$). More importantly, this order of magnitude implies that the cold wave crosses the 4 cm-long upstream inert zone in ~400s, which is consistent with the observed values of $t^{min}$ (between 200 s and 500 s). This order of magnitude corroborates the impact of the cold front propagation on the end of the backward movement.

### 3.3. Forward movement and asymptotic stabilization

As the cold thermal front keeps progressing, $\dot{Q}_{sens}$ exceeds $\dot{Q}_{reac}$ and the reaction front moves forward. It is clear from figure 6 that the general front velocity (global slope of $z_{front}(t)$ as long as one doesn't approach steady state) during the forward movement is a decreasing function of $T_{set}$.

The higher the value of $T_{set}$, the higher the thermal power released by the reaction (higher conversion of $CO_2$ into $CH_4$, in relation to the reaction rate increase with temperature – Arrhenius law). While lower than 1, $\dot{Q}_{react}/\dot{Q}_{sens}$ is higher at higher $T_{set}$, hence moderating the forward progression of the resulting wave (more negative value of $v_{chem}$).

Still, this first element of analysis doesn't give any information about how quickly the reaction front eventually stabilizes.

The characteristic times $T_{1/2}(T_{set})$ and $\tau(T_{set})$ as reported on figure 10.

Note that for $T_{set} = 410°C$, the duration of the experiment turned out to be insufficient for the front to be close enough to steady state: the local time is based on a final position that is significantly lower than the (unknown) asymptotic one, and the exponential approximation has difficulties fitting the experimental results. As a consequence, the points for experiment #3 underestimate significantly the real values. Whatever the real value, the fact that experience #3 has the longest characteristic times is sufficient to drive our analysis.

Figure 10 suggest that the start-up characteristic time reaches a maximum for a certain setpoint: for $T_{set} < T_{thres}$, the characteristic time of the front forward movement is an increasing function of $T_{set}$, while the characteristic time decreases with $T_{set}$ above $T_{thres}$.

It is reminded that if a cold inert gas was injected in a heated packed bed ($v_{chem} = 0$), the temperature front would move forward and $v_{ext}$ would be more and more negative until $v_{ext} = -v_{therm}$ at each location (profile stabilization). The corresponding characteristic time would be theoretically independent on the external temperature. In the present case, the characteristic time for the forward movement to stabilize also depends on the variations of $v_{chem}$ (value of $dv_{chem}/dt$, whether $|v_{chem}|$ is initially high or not). The existence of a maximum of the characteristic time as a function of $T_{set}$ suggests that two opposite mechanisms can come into play (3.3.1 and 3.3.2): $T_{thres}$ marks the limit between the respective predominance zones of the two mechanisms (mechanism 3.3.1 for $T_{set} < T_{thres}$ , mechanism 3.3.2 for $T_{set} > T_{thres}$).

### 3.3.1. Temperature gradient decrease

The cold front progression ends up when the whole inert porous zone of the reactor reaches the inlet gas temperature: the gas that reaches the reaction zone doesn't decrease in temperature anymore. Nevertheless, the reaction front keeps on moving with a local velocity $v_{front}$. During this progression, the temperature gradient of the front decreases: $\dot{Q}_{sens}$ decreases until $v_{reac}$ reaches $-(v_{therm} + v_{ext})$. The reaction zone located upstream the isothermal location (i.e. $z < z_T$) extends with the front progression. The residence time of the gas in this zone increases accordingly, which means that the reactants that reach $z_T$ are less and less pure as the front progresses.

This mechanism tends to delay the moment when $\dot{Q}_{reac}$ equilibrates $\dot{Q}_{sens}$, since the reaction rate at location $z_T$ decreases through time. The higher the temperature, the higher the consumption of reactants in the upstream zone of the reaction front. In other words, a high $T_{set}$ implies that $\dot{Q}_{reac}$ decreases almost as fast as $\dot{Q}_{sens}$ and the front stabilization is strongly delayed.

### 3.3.2. Positive thermochemical feedback and local temperature excursion

This mechanism is related to the existence of a positive thermal feedback between the temperature, the reaction rate, and the thermal power released by the reaction. Due to this feedback, the reaction rate can self-increase. One idealized way to model this behavior is to consider a theoretical situation where the reaction wouldn't trigger below a certain ignition temperature, and would be completed instantly above the ignition point. In this fictitious situation, the reactants would remain pure all along their movement in the cold upstream zone. As soon as they reach a point whose temperature is above ignition temperature, the reactants would be instantly converted, always releasing the whole reaction enthalpy $\dot{Q}_{ad}$ at a single location (reaction front = ignition front). The temperature variation at this ignition location would therefore follow the temperature variation of the upstream gas, but the ignition location would be constant. In other words, the cold front progression would imply a decrease in the ignition front temperature until the upstream gas reaches the inlet temperature (arrival of the cold front trailing edge); however, the front would stay immobile (no

forward movement, which means that the forward movement of the reaction front would have a duration of zero).

Of course, the real behavior of a reactor doesn't comply strictly with this binary ignition-based model. The deviation between the ignition-based model and reality is related to the fact that some conversion occurs before the gas reaches the sharp zone of the front: the heat released at the front isn't constant ($\dot{Q}_{reac}(z_T, t) < \dot{Q}_{ad}$), and the reaction front isn't infinitely steep. As the cold front progresses, the upstream zone of the reactor converts less and less reactants. Purer and purer reactants reach $z_T$, where $\dot{Q}_{reac}(z_T, t)$ increases and the reaction front gets steeper (as described in part 1.3). $v_{chem}(z_T, t)$ tends to be more and more negative, and opposes the positive component of $v_{front}$. To summarize, this mechanism implies that the higher the setpoint, the stronger the self-acceleration, the stronger the sharpening of the reaction front, and the sooner $v_{chem}$ becomes negative enough to stabilize the reaction front location.

## 4. Conclusion

The movement of the reaction front in a non-adiabatic pre-heated fixed-bed methanation reactor upon gas injection was investigated experimentally. It was shown that under the explored conditions, the hotspot moves back and forth before stabilizing in a downstream zone of the reactor (if the temperature setpoint is relatively low) or in an upstream zone (if the temperature setpoint is high). The instant-maximum velocity of the front backward movement turned out to be a linear function of the temperature setpoint. The start-up time seems to be a non-monotonous function of the setpoint, the maximum of the characteristic time being reached for the temperature setpoint threshold that separates the downstream/upstream stabilization frontier. It was shown that this behavior can be understood via the competition between the forward-moving thermal wave and the backward-moving chemical wave, the latter being dependent on the thermal and chemical conditions at the upstream vicinity of the reaction front.

Another noticeable point is that the hotspot movement follows the same qualitative behavior as the isothermal points. Even though the hotspot doesn't correspond to a given constant temperature, the fundamental governing mechanisms involved in its evolution are the same as those governing the evolution of an isothermal front: the hotspot properties are merely the result of the reaction front properties.

The observations made during the present experimental campaign were conducted with one gas flow rate only, the inlet gas mixture being stoichiometric. For future work, the same study should be conducted for different flow rates. The range of tested setpoints should be refined to check the reality of the threshold temperature existence, as well as its properties in terms of characteristic time. Relatively long time under operation should be chosen to let the reaction front position reach its quasi steady state.

If equipment modifications are possible, an improvement would consist in using more axial temperature measurement points, since the polynomial interpolation that was used here to establish the hotspot position is a source of uncertainties.

Alternatively or as a complement, a modelling & numerical simulation campaign would enable to access all the above-mentioned information. Different levels of complexity could be considered. A simple pseudo-homogeneous plug-flow model with quasi steady-state kinetics would give a first approximation. The difficulties are twofold. Firstly, the description of the catalytic medium isn't sufficient to predict the response of the system: the thermal behavior of the reactor wall, the tubing and the furnace can have a strong impact on the operation. Keeping the model simple despite these numerous elements would require numerous experiments to fit ad-hoc parameters with sufficient statistical representativeness. Secondly, the reproducibility of the experiments depends on the possibility of having precise timing (gas injection, composition measurement).

A more advanced modeling would use a multiscale model (pellet scale vs. bed scale) including the distribution of the diluted catalyst, which can play a significant role for highly diluted beds [31]. The obtention of transient kinetic laws is particularly difficult due to the coupling between the adsorption

effects and the reaction mechanisms ([32, 33]), but would result in further improvement in the accuracy of the predictions as quasi steady-state kinetics fail to capture some transient effects (e.g. delayed response of outlet water content [34]).

**Acknowledgement:** The authors thank Région Nouvelle Aquitaine, France, for funding this research.

**Conflict of interest:** The authors declare no conflict of interest

## Appendix A. Derivation of the front velocity equations

A simple model of a fixed-bed reactor (pseudo-homogeneous, 1D in axial direction, plug flow, no dispersion effect, constant thermophysical parameters and fluid velocity) leads to the following energy balance:

$$\left(\rho^{gas} \cdot C_p^{gas} + \rho^{solid} \cdot C_p^{solid}\right) \cdot \frac{\partial T}{\partial t} = -\rho^{gas} \cdot C_p^{gas} \cdot v_{gas} \cdot \frac{\partial T}{\partial z} + \dot{Q}_{reac} + \dot{Q}_{ext} \quad \text{(Eq. A.1)}$$

with $\dot{Q}_{reac} = -\Delta_r H \cdot r(C_i, T)$ the volumetric thermal power released by the reaction, and $\dot{Q}_{ext}$ the thermal power transferred from the outer surface of the reactor wall to the reaction medium (per unit of reaction medium volume).

Equation A.1 can be rewritten:

$$-\left(\frac{\partial T}{\partial t}\right) \cdot \left(\frac{\partial T}{\partial z}\right)^{-1} = \frac{\rho^{gas} \cdot C_p^{gas}}{\rho^{gas} \cdot C_p^{gas} + \rho^{solid} \cdot C_p^{solid}} \cdot v_{gas} - \frac{\dot{Q}_{reac} + \dot{Q}_{ext}}{\rho^{gas} \cdot C_p^{gas} + \rho^{solid} \cdot C_p^{solid}} \cdot \left(\frac{\partial T}{\partial z}\right)^{-1} \quad \text{(Eq. A.2)}$$

A moving point whose temperature is $T$ (constant) travels a distance $dz_T$ during the time interval $dt$ (figure A.1), such that:

$$dT = 0 = \frac{\partial T}{\partial t} dt + \frac{\partial T}{\partial z} dz_T \quad \text{(Eq. A.3)}$$

Hence, the phase velocity of the corresponding wave (velocity of an isothermal point in Lagrangian description) is:

$$v_T = \frac{dz_T}{dt} = -\left(\frac{\partial T}{\partial t}\right) \cdot \left(\frac{\partial T}{\partial z}\right)^{-1} \quad \text{(Eq. A.4)}$$

Equation A.2 becomes:

$v_T = v_{therm} + v_{chem} + v_{ext}$ (Eq. A.5)

with $v_{therm} = \frac{\rho^{gas} \cdot C_p^{gas}}{\rho^{gas} \cdot C_p^{gas} + \rho^{solid} \cdot C_p^{solid}} \cdot v_{gas}$

$v_{chem} = -\frac{\dot{Q}_{reac}}{\rho^{gas} \cdot C_p^{gas} + \rho^{solid} \cdot C_p^{solid}} \cdot \left(\frac{\partial T}{\partial z}\right)^{-1} \times \left(\frac{\rho^{gas} \cdot C_p^{gas} \cdot v_{gas}}{\rho^{gas} \cdot C_p^{gas} \cdot v_{gas}}\right) = -\frac{\dot{Q}_{reac}}{\dot{Q}_{sens}} \cdot v_{therm}$

and $v_{ext} = -\frac{\dot{Q}_{ext}}{\rho^{gas} \cdot C_p^{gas} + \rho^{solid} \cdot C_p^{solid}} \cdot \left(\frac{\partial T}{\partial z}\right)^{-1} \times \left(\frac{\rho^{gas} \cdot C_p^{gas} \cdot v_{gas}}{\rho^{gas} \cdot C_p^{gas} \cdot v_{gas}}\right) = -\frac{\dot{Q}_{ext}}{\dot{Q}_{sens}} \cdot v_{therm}$

**Appendix B. Building the equivalent exponential function**

Aside from the integral approach used in this paper, the "equivalent exponential function" can be obtained thanks to various strategies. For example, one can minimize the RMS function of the difference between the experimental value and the equivalent function (equation B.1).

$$RMS^2(z_{hot}) = \frac{1}{n} \cdot \sum_i \left[z_i - \left(z_{hot}^{min} + \left(z_{hot}^{\infty} - z_{hot}^{min}\right) \cdot \left(1 - \exp\left(-\frac{t_i - t^{min}}{\tau}\right)\right)\right)\right]^2 \quad \text{(Eq. B.1)}$$

with $z_i$ the location of the hotspot at instant $t_i$ ($n$ measurements from $t^{min}$ to the end of the experiment).

A variation of this method is to minimize the function defined by equation B.2:

$$RMS^2(t \cdot z_{hot}) = \frac{1}{n_i} \cdot \sum_i t_i^2 \cdot \left[z_i - \left(z_{hot}^{min} + \left(z_{hot}^{\infty} - z_{hot}^{min}\right) \cdot \left(1 - \exp\left(-\frac{t_i - t^{min}}{\tau}\right)\right)\right)\right]^2 \quad \text{(Eq. B.2)}$$

The equivalent exponential obtained by means of the $RMS^2(t \cdot z_{hot})$ captures the asymptotic slope of the experimental results with more accuracy than the equivalent exponential based on $RMS^2(z_{hot})$. However, $RMS^2(t \cdot z_{hot})$ does not capture the early part of the transition as well as $RMS^2(z_{hot})$.

It should be noticed that the minimization of $RMS^2(z_{hot})$ or $RMS^2(t \cdot z_{hot})$ with $\tau$ as unique variable requires the accurate knowledge of $z_{hot}^{\infty}$, which can be hard if the experiment duration can't guarantee that steady state will be reached. Alternatively, one can minimize $RMS^2$ as a function of the two variables $\{z_{hot}^{\infty}, \tau\}$ , which requires more computation effort. This point enlightens the

advantage of the integral-based derivation of the equivalent exponential: $\tau$ can be determined without any knowledge of $z_{hot}^{\infty}$, and $z_{hot}^{\infty}$ can be calculated *a posteriori* to check if is matches the experimental results.

Whatever the approach used, the $\tau$ corresponding to the various experiments of this study turned-out to remain relatively unchanged. Figures B.1 and B.2 compare the three different approaches (integral, $RMS^2(z_{hot})$ and $RMS^2(t \cdot z_{hot})$).

The equivalent exponential curve is shown on figure B.1 for two extreme cases:

- for $T_{set} = 440°C$, the experimental curve is very similar to a real exponential, so the results of the various approaches are nearly indistinguishable.
- for $T_{set} = 400°C$ , the deviation from an exponential function is the most prominent. Even in this "worst-case scenario", the exponential approximations are relatively similar.

Figure B.2 reports the $\tau$ associated to the various methods for each $Tset$. The $z_{hot}^{\infty}$ value were obtained together with $\tau$ in the case of $RMS^2$, and was calculated *a posteriori* in the integral case.

## References


1. Riese J., Grünewald M. Challenges and Opportunities to Enhance Flexibility in Design and Operation of Chemical Processes. Chemie Ingenieur Technik 92 No. 12 (2020), pp.1-12. DOI : 10.1002/cite.202000057

2. Bremer J., Sundmacher K. Operation Range Extension via Hot-Spot Control for Catalytic $CO_2$ Methanation Reactors. Reaction Chemistry & Engineering 4 (2019), pp. 1019-1037. DOI : 10.1039/C9RE00147F

3. Fischer K. L., Freund H. Intensification of Load Flexible Fixed Bed Reactors by Optimal Design of Staged Reactor Setups. Chemical Engineering and Processing (2020). DOI : 10.1016/j.cep.2020.108183

4. Bremer J., Rätze H. G., Sundmacher K. $CO_2$ Methanation : Optimal Start-Up Control of a Fixed-Bed Reactor for Power-to-Gas Applications. AIChE journal vol. 63-1 (2017), pp. 23-31. DOI : 10.1002/aic.15496.

5. Crider J.E., Foss A.S. Computational studies of transients in packed tubular chemical reactors. AIChE Journal vol. 12-3 (1966), pp. 514-522. DOI : 10.1002/aic.690120322

6. Try R., Bengaouer A., Baurens P., Jallut C. Dynamic modeling and simulations of the behavior of a fixed-bed reactor-exchanger used for CO2 methanation. AIChE Journal vol. 64-2 (2017). DOI : 10.1002/aic.15874

7. Sharma C. S., Hughes R. The behaviour of an adiabatic fixed bed reactor for the oxidation of carbon monoxide-I. Chemical engineering science vol. 34 (1979), pp. 613-624.

8. Sharma C. S., Hughes R. The behaviour of an adiabatic fixed bed reactor for the oxidation of carbon monoxide-II. Chemical engineering science vol. 34 (1979), pp. 625-634.

9. Van Doesburg H., De Jong W. A. Transient behaviour of an adiabatic fixed bed methanator I – Experiments with binary feeds of CO or CO2 in hydrogen. Chemical engineering science vol. 31 (1976), pp. 45-51.

10. Lehr C. G., Yurchak S., Kabel R. L. Response of a tubular heterogeneous catalytic reactor to a step increase in flow rate. AIChE Journal vol. 14-4 (1967), pp. 627-636.

11. Try R. Étude expérimentale et modélisation dynamique d'un réacteur catalytique modulaire pour l'hydrogénation du CO2 en méthane. Ph.D dissertation (2018), Université Claude Bernard Lyon 1.

12. Stangeland B.E., Foss A.S. Control of a fixed-bed chemical reactor. Industrial & engineering chemistry fundamentals vol. 9-1 (1970), pp. 38-48.

13. Sheintuch M. Excitable waves in a fixed bed reactor : observations and analysis. Chemical engineering science vol. 45-8 (1990), pp. 2125-2132.

14. Gatica J.E., Puszynski J., Hlavacek V. Reaction front propagation in nonadiabatic exothermic reaction flow systems. AIChE Journal Vol. 33-5 (1987).

15. Sheintuch M., Adjaye J. Excitable waves in a fixed bed reactor : ethylene oxidation on platinum. Chemical engineering science vol. 45-7 (1990), pp. 1897-1903.

16. Puszynski J., Hlavacek V. Experimental study of traveling waves in nonadiabatic fixed bed reactors for the oxidation of carbon monoxide. Chemical engineering science vol. 33 (1979), pp. 1769-1774.

17. Jensen K. F., Ray W.H. The bifurcation behavior of tubular reactors. Chemical engineering science vol. 37-2(1982), pp. 199-222. DOI: 10.1016/0009-2509(82)80155-3

18. Yakhnin V., Menzinger M. High temperature transients in catalytic fixed-bed reactors. Reviews in chemical engineering 20 vol. 3-4 (2004). DOI : 10.1515/REVCE.2004.20.3-4.175

19. Yakhnin V.Z., Menzinger M. Moving hot spots and resonance in adiabatic packed-bed reactors. AIChE Journal 44-5 (1998).

20. Li Q., Chen G., Zhu Y., Li X., Yao Y. Resonance response in the catalytic combustion of methane and propane binary mixture in reverse-flow reactor.Chemical Engineering Journal 345 (2018), pp. 375-388. DOI : 10.1016/j.cej.2018.03.165

21. Altimari P., Mancusi E., Crescitelli S. Formation of thermal wave trains in loop reactors: stability limits and spatiotemporal structure for reversible reactions. Industrial & engineering chemistry research 51 (2012), pp. 9609-9619. DOI : 10.1021/ie2030008

22. Lee W.J., Li C., Prajitno H., Yoo J., Patel J., Yang Y., Lim S. Recent trend in thermal catalytic low temperature CO2 methanation : a critical review. Catalysis today (2020). DOI : 10.1016/j.cattod.2020.02.017

23. Fache A., Marias F., Guerre V., Palmade S. Intermittent operation of fixed-bed methanation reactors: a simple relation between start-up time and idle state duration. Waste and Biomass, Valorization 11 (2018), pp. 447–463. DOI : 10.1007/s12649-018-0507-3

24. Narendiran K., Viswanathan G. A. Impact of Wall Heat Transport on Formation of Transversal Hot Zones in Shallow, Non-adiabatic Packed-Bed Reactors. Industrial & engineering chemistry research 54 (2015), pp. 7352-7363. DOI: 10.1021/acs.iecr.5b01048

25. Marwaha B., Luss D. Hot zones formation in packed bed reactors. Chemical engineering science vol. 58 (2003), pp. 733-738. DOI : 10.1016/S0009-2509(02)00602-4

26. Partopour B., Dixon A. G. Integrated multiscale modeling of fixed bed reactors: studying the reactor under dynamic reaction conditions. Chemical engineering journal (2018). DOI: 10.1016/j.cej.2018.08.124

27. Vortmeyer D., Jahnel W. Moving reaction zones in fixed bed reactors under the influence of various parameters. Chemical engineering science vol. 27-8 (1972), pp. 1485-1496.

28. Zahn V. M. Adiabatic simulated moving bed reactor – principle, nonlinear analysis and experimental demonstration. Dr.-Ing. dissertation (2012) of Otto von Guericke Universität, Magdeburg. https://pure.mpg.de/rest/items/item_1752935/component/file_1752934/content accessed December 30 2020.

29. Lugo-Pimentel M. A. A thin layered structural coating on a metal substrate for enhanced hydrogen production from steam methane reforming. M.Sc. dissertation (2017) of City University of New-York.

30. Pita J., Balakotaiah V., Luss D. Thermoflow multiplicity in a packed-bed reactor: Conduction and cooling effects. AIChE journal vol. 35-3 (1989), pp. 373-384. DOI : 10.1002/aic.690350305.

31. Berger R. J., Pérez-Ramirez J., Kapteijn F., Moulijn J. Catalyst performance testing: bed dilution revisited. Chemical Engineering Science 57 (2002), pp. 4921-4932. DOI : 10.1016/S0009-2509(02)00273-7

32. Bundhoo A., Schweicher J., Frennet A., Kruse N. Chemical Transient Kinetics Applied to CO Hydrogenation over a Pure Nickel Catalyst. Journal of Physical Chemistry C 113, 24 (2009), pp. 10731-10739. DOI : 10.1021/jp902647z

33. Vesselli E., Schweicher J., Bundhoo A., Frennet A., Kruse N. Catalytic $CO_2$ Hydrogenation on Nickel: Novel Insight by Chemical Transient Kinetics. Journal of Physical Chemistry C 115, 4 (2011), pp. 1255-1260. DOI : 10.1021/jp106551r

34. Tauer G., Kern C., Jess A. Transient Effects during Dynamic Operation of a Wall-Cooled Fixed-Bed Reactor for CO 2 Methanation. Chemical Engineering & Technology Vol. 42-11 (2019). DOI : 10.1002/ceat.201900367

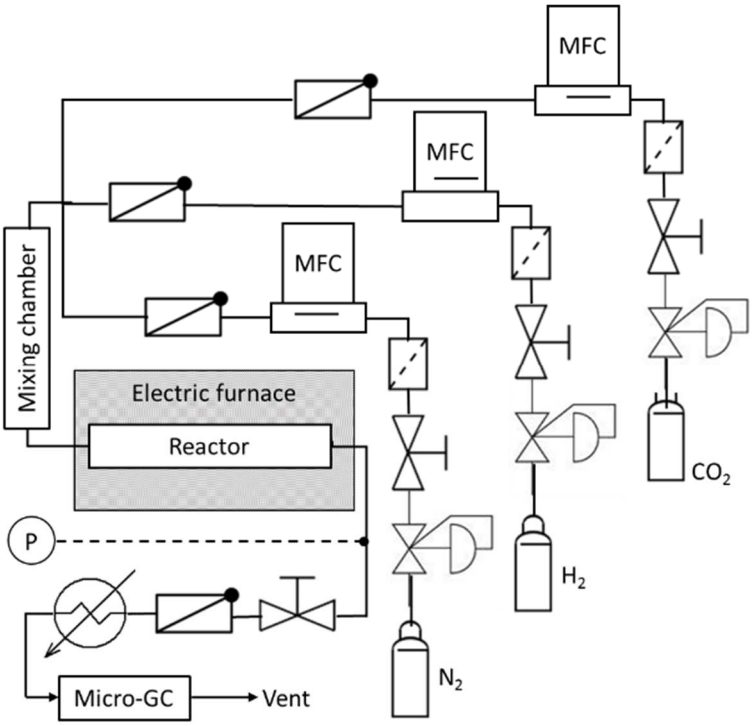


Figure 1. General schematic of the experimental setup.

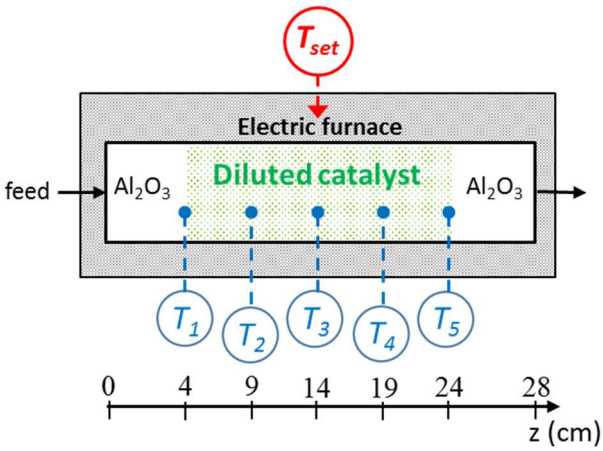


Figure 2. Temperature measurement in the reactor, and temperature control in the furnace.

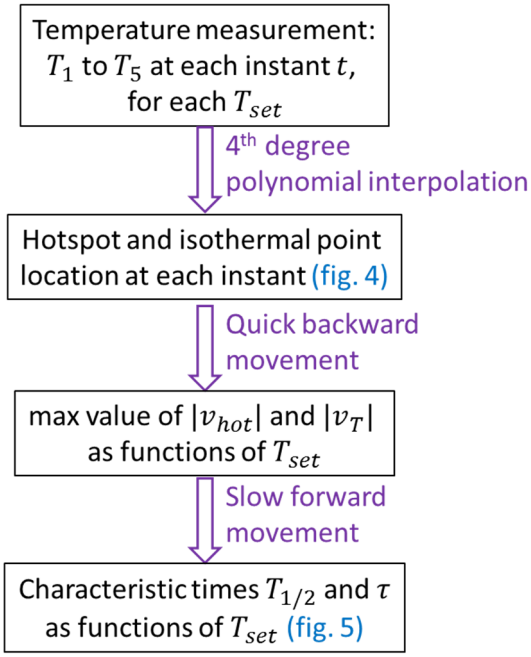


Figure 3. Post treatment procedure: from raw temperature measurements to velocities and characteristic times determination.

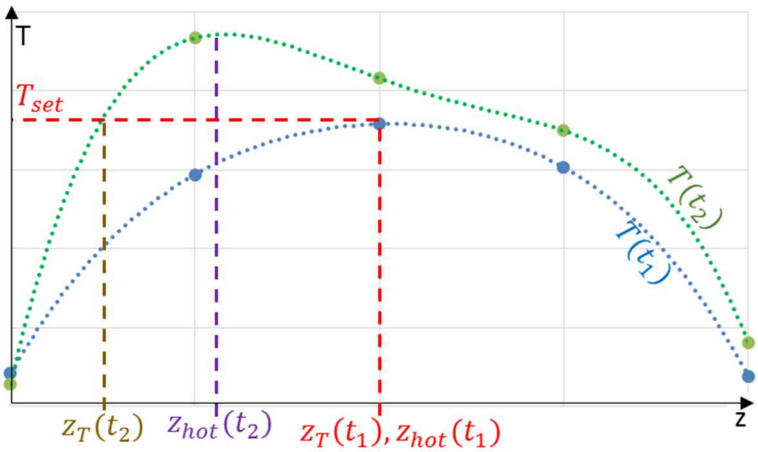


Figure 4. Polynomial interpolation and determination of the locations of the isothermal point ($z_T; T = T_{set}$) and of the hotspot ($z_{hot}; \partial T/\partial z = 0$) at two different instants $t_1$ and $t_2$ (qualitative typical example). $z_T$ and $z_{hot}$ are considered as two indicators of the reaction front movement.

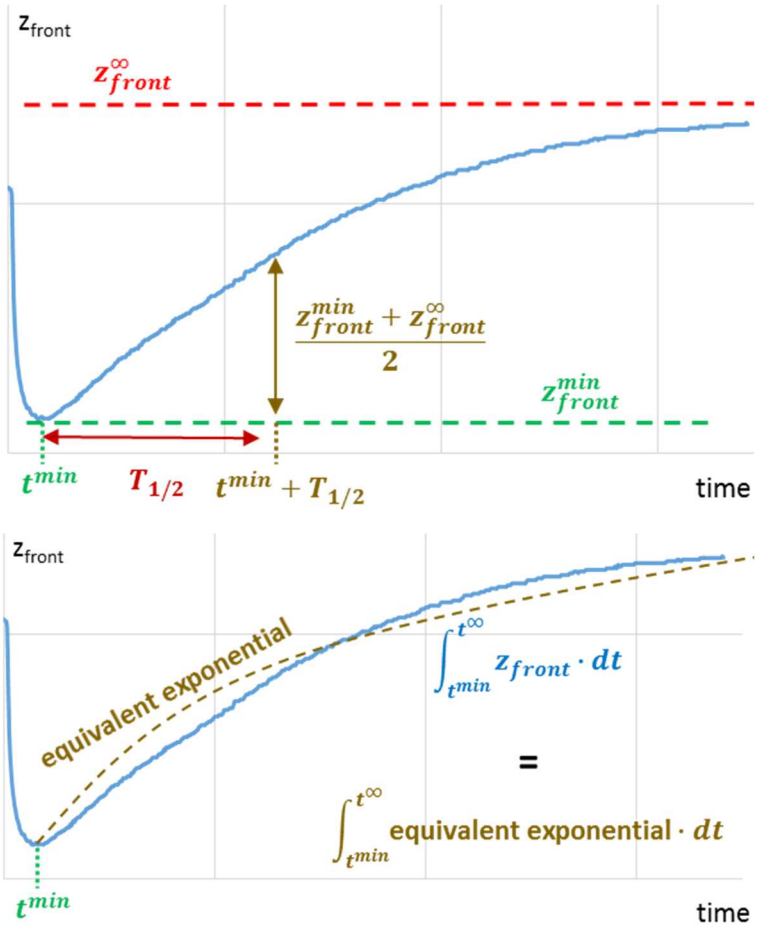


Figure 5. Evolution of the front location upon gas injection (qualitative typical example). Local characteristic time (top) and definition of the equivalent exponential function for the integral characteristic time (bottom).

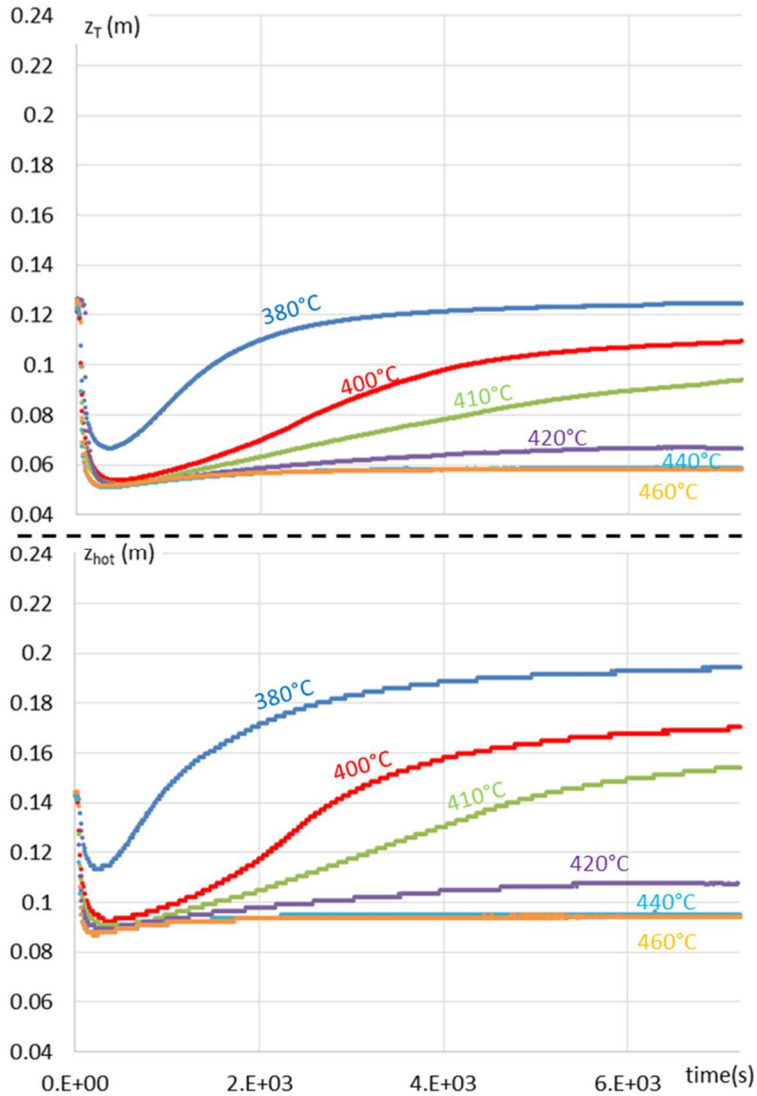


Figure 6. Evolution of the reaction front upon gas injection, for the six values of $T_{set}$: $z_T(t)$ (top) and $z_{hot}(t)$ (bottom). It is reminded that the reaction zone extends from z = 4 cm to z = 24 cm.

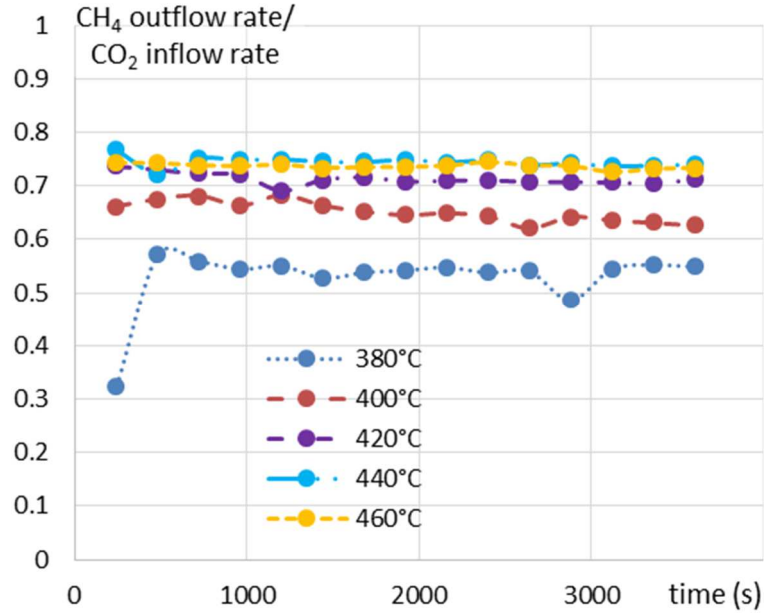


Figure 7. Conversion of $CO_2$ into methane upon gas injection (lines are shown to ease readability).

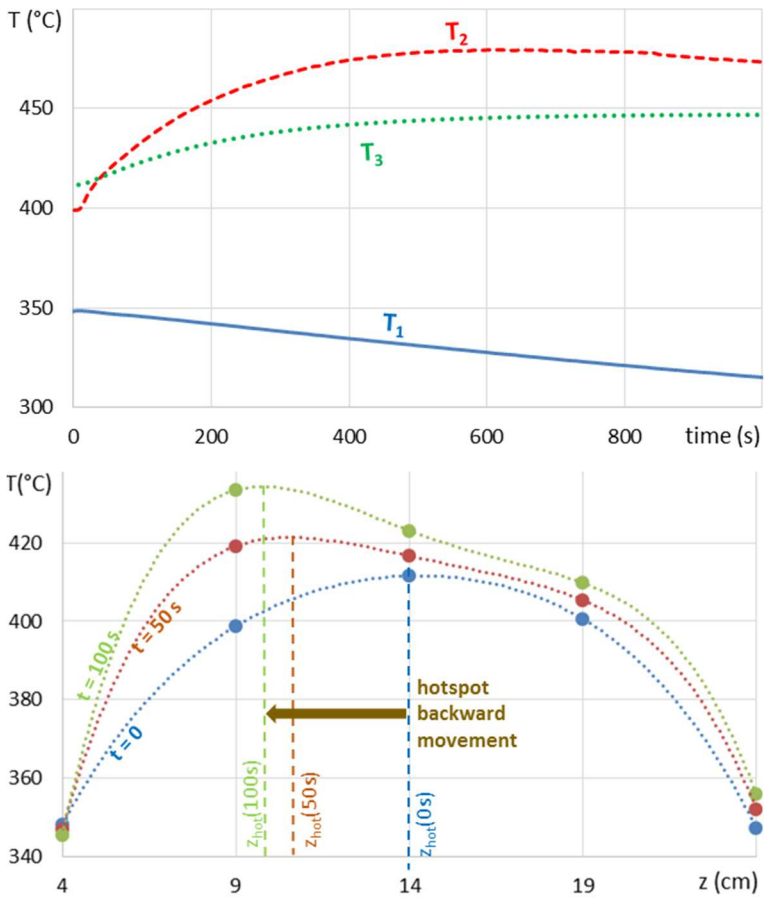


Figure 8. Evolution of temperatures $T_1$ to $T_3$ upon gas injection (top) and evolution of the hotspot location (bottom), when $T_{set} = 410°C$.

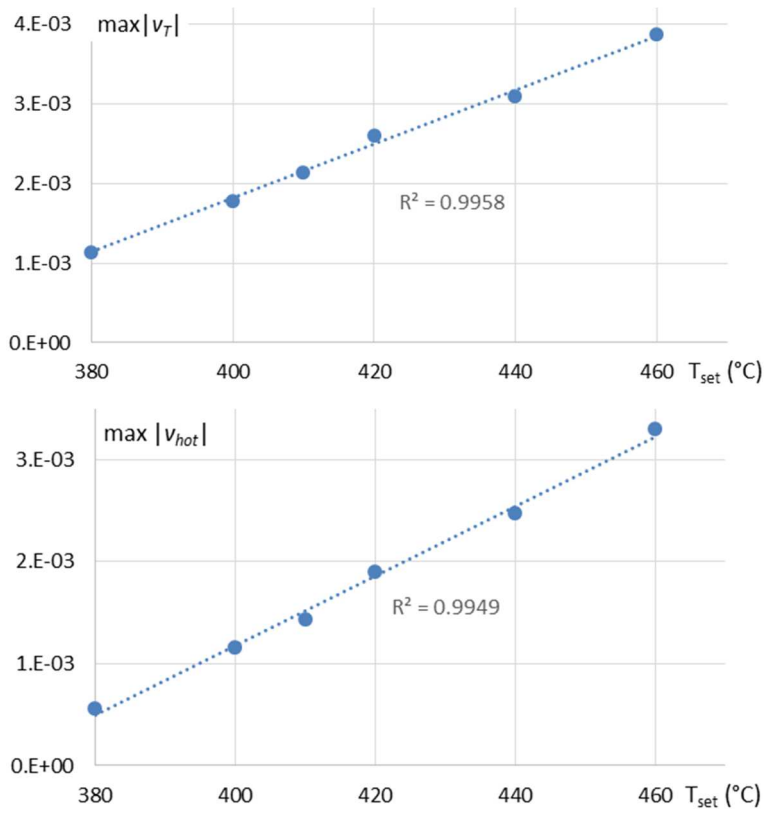


Figure 9. Maximum value of the front backward velocity as a function of the setpoint temperature (top: isothermal, bottom: hotspot).

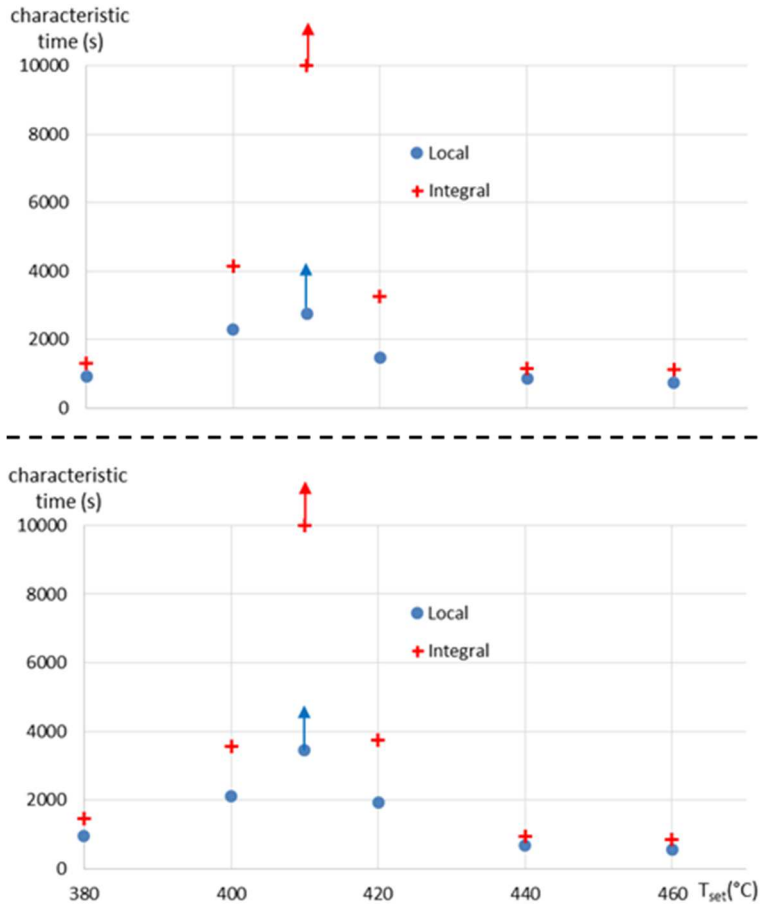


Figure 10. Characteristic times $T_{1/2}$ (local) and $\tau$ (integral) of the front downstream movement as a function of the temperature setpoint (top = isothermal, bottom = hotspot). The arrows indicate that the characteristic times couldn't be determined accurately for $T_{set} = 410°C$ (too much time required to reach steady state), but they are higher than the reported values.

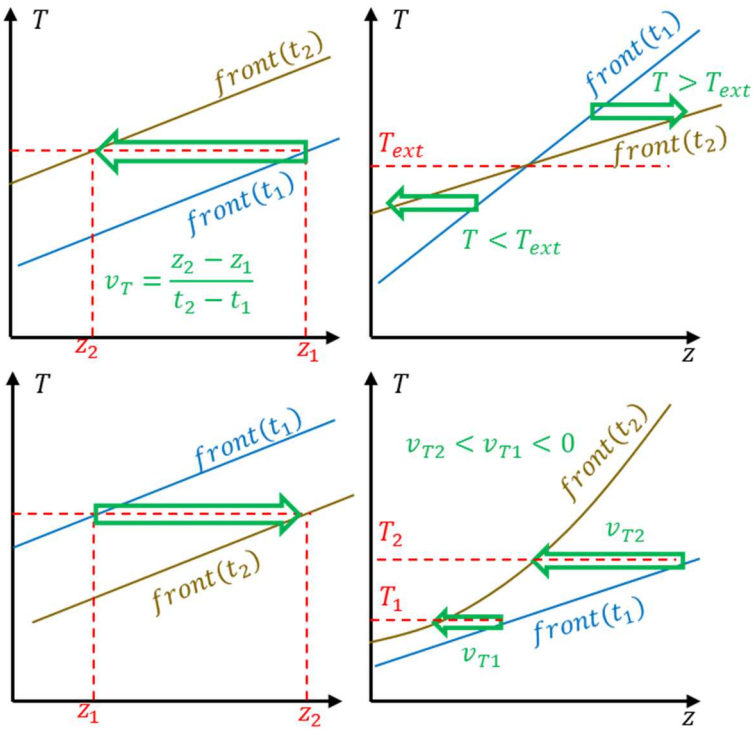


Figure A.1 Relocation of an isothermal point during a temperature variation of the reaction front.
Left: the front is linear and stays parallel to itself (spatially uniform thermal powers, or local linearization). Top (bottom, resp.): $\dot{Q}_{reac} > \dot{Q}_{sens}$ ($\dot{Q}_{reac} < \dot{Q}_{sens}$ resp.).
Right: $v_T$ isn't uniform. Top: the front rotates due to external heat exchange. Bottom: the impact of the temperature increase on the reaction rate exceeds that of the reactants consumption ($\partial \dot{Q}_{reac}/\partial z > 0$).

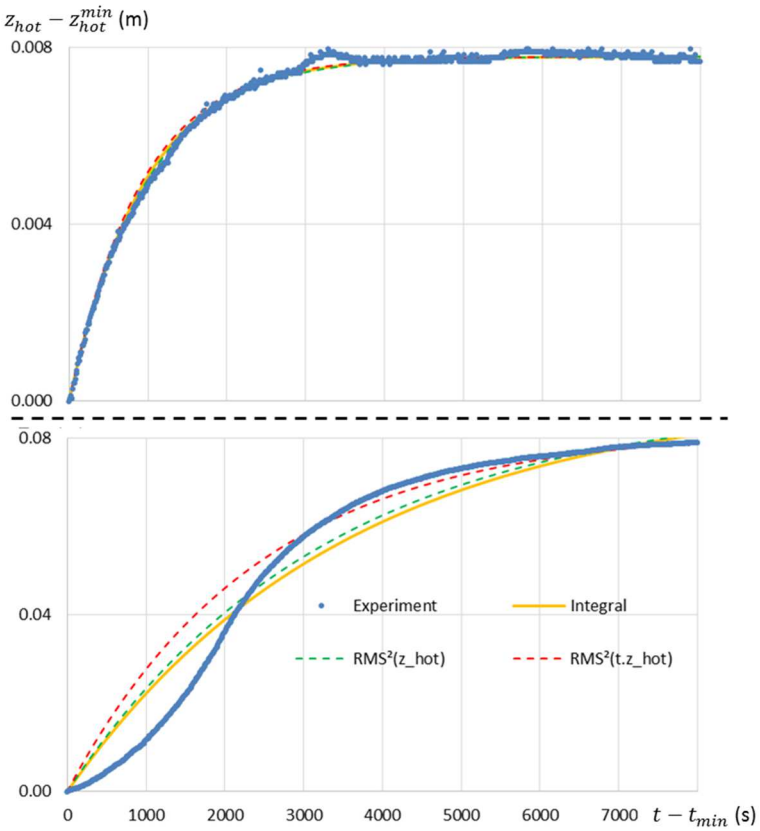


Figure B.1 Comparison of the equivalent exponential functions obtained by three different methods to the experimental results, for $T_{set}$ = 440°C (top) and $T_{set} = 400°C$ (bottom). The position is offset so the 0 value of the graph corresponds to $\{t^{min}, z_{hot}^{min}\}$ for each experiment.

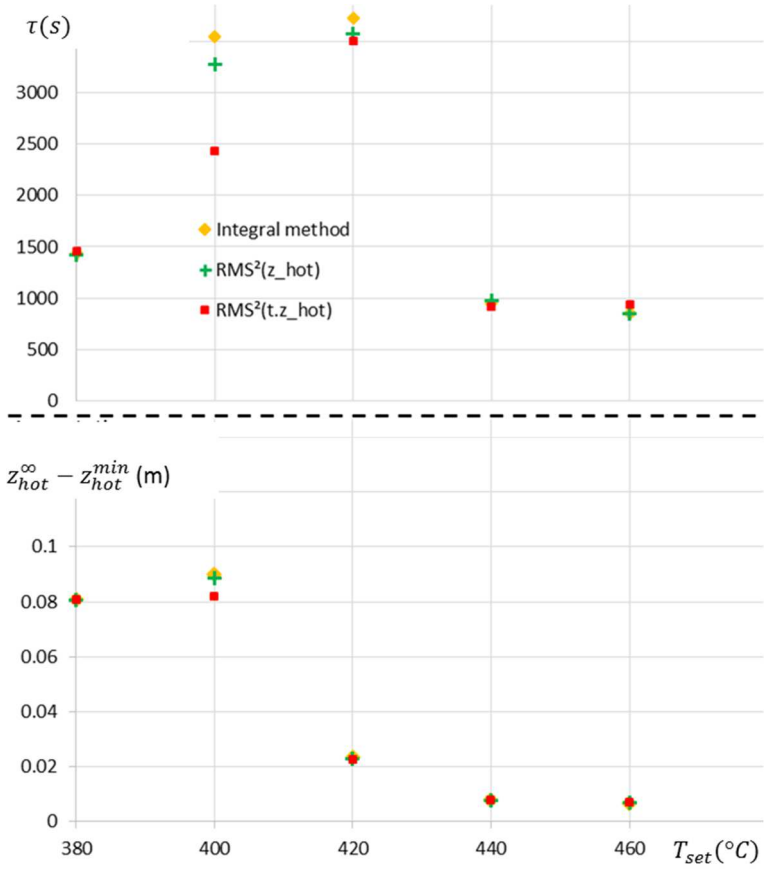


Figure B.2 Comparison of the $\{\tau, z_{hot}^{\infty}\}$ obtained by three different methods. The values for $T_{set} = 410°C$ are not reported because the only relevant available information is that the corresponding $\tau$ is too long to be determined.

| Load # | Catalyst mass | Alumina mass |
|---|---|---|
| outlet zone | 0 | 6.007 |
| 1 | 0.1521 | 2.9483 |
| 2 | 0.1527 | 2.8308 |
| 3 | 0.1494 | 2.8625 |
| 4 | 0.1580 | 2.8570 |
| 5 | 0.1455 | 2.8520 |
| 6 | 0.1545 | 2.8706 |
| 7 | 0.1563 | 2.8760 |
| 8 | 0.1507 | 2.8651 |
| 9 | 0.1533 | 2.8545 |
| 10 | 0.1527 | 2.8740 |
| inlet zone | 0 | 6.0535 |

Table 1. Partial loads of the reactor. Masses are expressed in grams.

| Experiment # | $T_{set}$ (°C) |
|---|---|
| 1 | 380 |
| 2 | 400 |
| 3 | 410 |
| 4 | 420 |
| 5 | 440 |
| 6 | 460 |

Table 2. Temperature setpoint of the experiments.